Deep Learning:
Automated Surface Characterization of Porous Media to Understand Geological Fluid Flow

Wonjin Yun
Stanford University
wyun@stanford.edu

Abstract

In this paper, FCN and CNN were trained on the image data set that were prepared from the in-house fabricated micro-fluidic device and fluid injection experiment. Trained FCN and CNN model provide the best validation accuracy of 0.81 and 0.83, respectively, for the surface wettability classification of sandstone and carbonate pore structure.

1. Introduction

Energy underpins all aspects of modern life. Energy use is directly correlated with broad measures of societal health including the human development index, and female life expectance at birth more is more. Human ingenuity, innovation and technology has been focusing on relieved the greater pressure on worlds energy demand allowing people to gain more access to energy and to power their higher standards of living.

In many of the challenges we face today as geoscientists, in particular in the context of water and energy resources, fluid invasion into a porous soil or sediment is a key process in different scale ranged from pore to reservoir scale shown in Fig.1. Examples include hydrocarbon migration and recovery, methane venting from hydrate-bearing sediments, drying and wetting of soils, and carbon geosequestration.

Complex interplay between capillary, viscous, and gravitational forces, wettability effects, and the underlying heterogenous pore geometry, leads to ramified, preferential flow paths.Particularly, Fig.1 demonstrate the key mechanism at pore-scale where oil invade into narrower pore throat (R_{th}) when pressure difference ($P_1 - P_2$) is higher than the capillary pressure ($2 * \sigma * (\frac{1}{R_{th}} - \frac{1}{R_b})$). Here, σ interfacial tension that is strongly related with the surface wettability.

$$P_1 - P_2 \quad > \quad 2 * \sigma * (\frac{1}{R_{th}} - \frac{1}{R_b})$$

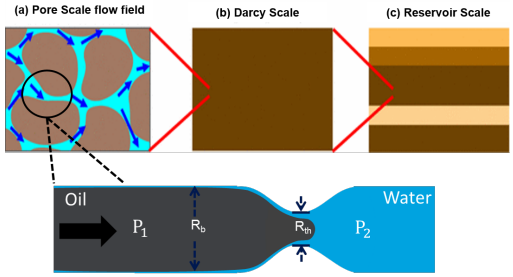

Figure 1. Schematic diagram of fluid invasion into a porous soil or sediment at different scale from pore to reservoir scale.

Hence, the microscale visualization of fluids in complex geometry brings better understanding of fluid movement, droplet generation and other effects, especially for the effect of wettability of the surface geometry on fluid flow.[8] The effect of wettability, simply oil-wet and water-wet shown in Fig.2 , on the fluid movement can be studied, visualized and modeled on a micro-level representative of the actual rock structure, so called micromodel. Micromodel is a silicon-based microfluidic device that are particularly useful laboratory tools for the direct visualization and image acquisition of fluid flow revealing mechanisms controlling flow and transport phenomena in natural porous media [7][6]. Microscopic image in Fig.2 demonstrate fluid saturation patterns for oil or water-wet condition of sandstone-like pore geometry.

1.1. Challenges

Predicting the emergent patterns is challenging, because of the sensitivity to pore-scale details and the large number of coupled mechanisms and governing parameters which vary over a wide range of values and scales. To evaluate the variability of multi-phase flow properties of porous media at the pore scale, it is necessary to acquire a large number of representative samples of the void-solid structure. Indeed, image analysis on microscopic images requires tremendous

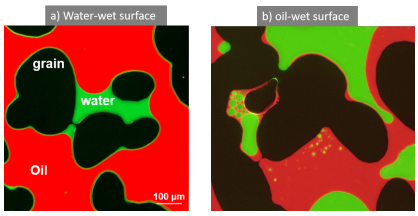

Figure 2. a) Example image of oil and water in the micromodel with water-wet surface. Water-wet can be shown as the water (green) surrounds the grain (black). Capillary pressure forces the wetting-phase (water) to occupy the smaller spaces than the pore spaces occupied by oil (red). The shape of interface between oil and water tells the water-wet characteristic of surface. b) Image of oil and water in the micromodel with oil-wet surface that the oil (red) surrounds the grain (black) and occupies the smaller spaces than the pore spaces occupied by water (red).

time effort.

1.2. Problem Statement

Hence, application of Convolutional Neural Networks should be achieved for automated surface-wettability classification of massive microscopic pore scala images from core scale domain.

2. Related Work

Deep learning allows computational models that are composed of multiple processing layers to learn representations of data with multiple levels of abstraction. These methods have dramatically improved the state-of-the-art in speech recognition, visual object recognition, object detection and many other domains such as drug discovery and genomics.[3] However, there have not been many studies applying the deep learning technique to geology or energy-fluid system.

As mentioned, it is necessary to acquire a number of representative samples of the void-solid structure for reliable evaluation of the variability of multi-phase flow properties of porous media at the pore scale. Recently, Mosser *et al*. (2017) [4] present a novel method to reconstruct the solid-void structure of porous media by applying a generative neural network (GAN). By using an adversarial learning approach for neural networks, the authors were able to generate representative samples of porous media at different scales that are representative of the morphology of a bead pack, Berea sand-stone, and Ketton limestone.

Here, this report will discuss both experimental procedure to produce massive pore scale images and the application of deep learning including Fully Connecte Layer Network, Convolutional Network, AlexNet[2] to perform the classification of wettability of pore structure in micromodel device.

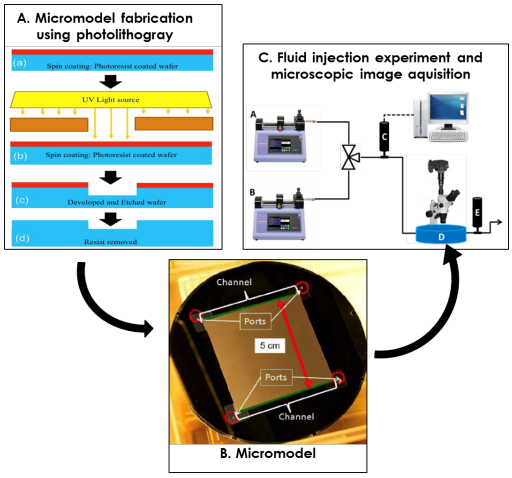

Figure 3. Schematic illustration of micromodel fabrication (A) and the use of micromodel(B). Experimental set-up for fluid injection (C) for producing image data is demonstrated.

3. Data Acquisition Process

This section will discuss the experimental procedure to fabricate the microfluidic device with oil- and water-wet properties and the use of laser scanning fluorescence microscope (LSFM) to generate pore scale images.

3.1. Micromodel manufacturing

Micromodel fabrication takes place in the Stanford Nanofabrication Facility (SNF). As showin in Fig.3A and Fig.3B, 4-inch silicon wafers were etched to create the pore network on the wafer surface. Finally, a glass cover plate was bonded to the top of the etched wafer in order to contain the fluid in the pore channels that were etched on the silicon water surface. Initially, the silicon wafer surface is water-wet and the surface was modified to oil-wet by silane modification process using hexamethyldisilazane (HMDS). [1] Microfluidic devices will have four different rock patterns: sandstone-A and carbonate and the surface wettability of each rock pattern is both oil-wet and water-wet.

3.2. Microscopic image acquisition

Two different phases, *e.g*. mineral oil and water, were injected into microfluidic devices shown in Fig.3C. Image will be taken and visualize the saturation profile of two phase in complex geometry. Image acquisition will be conducted using the laser scanning fluorescence microscope (LSFM) with 100X objectives magnification. Field of veiw (FOV) of a single image is about the size of 800 μm by 800μm. The importance of the size of FOV during the training the neural network will be discussed in section.4.1.

Raw pixel data (200×200×3 pixels) of images with the corresponding pixel-wise fluorescence emission wave-

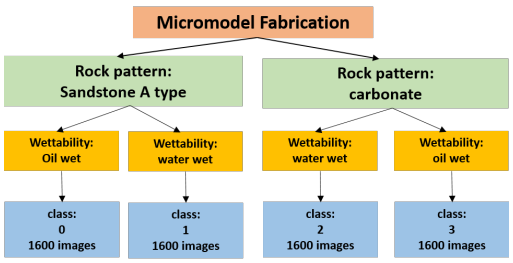

Figure 4. Diagram of the structure of dataset.

length data will be utilized for the post-image processing. After the post-image processing, the phases including mineral oil, water, and grain (pore structure) in the images were identified and labeled. 1600 images for each class per rock pattern will be prepared with their classes as shown in Fig.4.

4. Data and Preprocessing

We will examine 6400 microscopic images with different FOV for four classes.

4.1. Variation of spacial resolution

In Fig.5 and Fig.6, training image data set has four different spacial resolution (0.6x, 1x, 2x, and 3x) via zoom-operation of LSFM image capture. From the baseline FOV (800μm by 800μm) of 1x-zoom, 0.6x-zoom increases the size of FOV ;and 2x and 3x-zoom decrease the size of FOV. Hence, 0.6x-zoom is particularly useful for overview the distribution of two-phases in the large area of pore network, however, it gives not enough resolution of showing thin-film surrounding grain (black). On the other hand, 3x-zoom provides the image with high-resolution details of thin-film and the shape of interfacial curvature for wettability classification. In turn, the training images with combining four different spacial resolutions are helpful to promote validation or test accuracy of CNN network. In contrast to the sandstone with relatively uniformly distributed pore and grain, varying spacial resolution should be beneficial for pore network, especially the carbonate with very high heterogeneity of pore and grain size distribution,

4.2. Data structure

The dataset consists of 6400 200x200 color images in 4 classes for sandstone and carbonate rock pattern, with 1600 images per class. 400 images per each zoom-level were taken. There are 1500 training images and 100 test images per each class. The dataset has been post-processed to be stored as a file with name of *data-batch-1* with 6300 images and *test-batch* with 100 images. The test batch contains exactly 100 randomly-selected images from each class. The training batches contain the remaining images in random

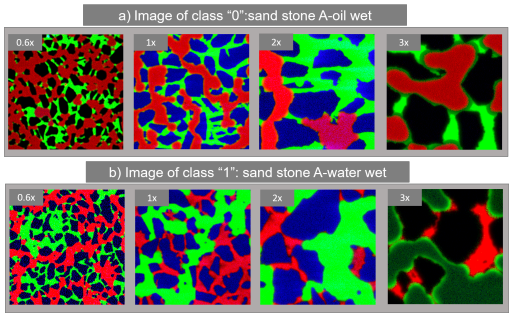

Figure 5. Example of training images of class "0:sandstone A-oilwet" and "1:sandstone A-waterwet". Four different size (1x, 0.6x, 2x, and 3x) of FOV per class are shown

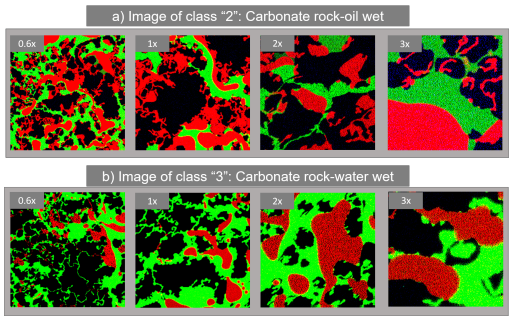

Figure 6. Example of training images of class "2:carbonate-oilwet" and "3:carbonate-waterwet". Four different size (1x, 0.6x, 2x, and 3x) of FOV per class are shown.

order.Fig.5 and Fig.6 shows the example of training image in the *data-batch-1*.

5. Method

We treat our problem as supervised regression and tackle this problem by convolutional neural network models. In this section, we discussed our models in details and also talked about evaluation criteria.

5.1. Fully-Connected Neural Nets (FCN)

Following the assignment2 of the course material, a fully-connected neural network with an hidden layers of [512, 256, 128, 128], ReLU nonlinearities, and a softmax loss function. The model implemented dropout(=0.5) and batch normalization. For a network with 5 layers, the hyper-parameters are regularization (= 1e-4), update rule(rmsprop), and learning rate (=2e-4) with number of epochs(=15) and batch size of 128.

5.2. Convolutional Networks (CNN)

A three-layer convolutional network with the following architecture in Table.2 with an hidden layers of 500 dimension, ReLU nonlinearities,maxpool, and a softmax loss

Table 1. Summary of Model

Model	Architecture
FCN	(affine-batchnorm-relu-dropout) ×(L-1)-affine-softmax
CNN	conv-relu-2×2 maxpool -affine-relu-affine-softmax

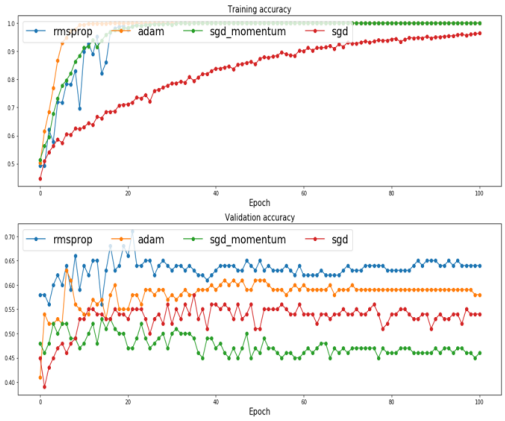

Figure 7. Evaluation of update rule with FCN architecture using 1000 image data of Sandstone rock type only.

function. The hyper-parameters are regularization (= 1e-1), update rule(adam), and learning rate (=2e-4) with number of epochs(=15) and batch size of 50.

6. Result and Discussion

The wettability and the shape of pore structure is the factor to change the ganglia shape of oil and water and determine the occupation of each phase in difference size of pore. The goal of the project is to predict the wettability (oil or water wet) for the given test images that has the oil and water phases with pore space.

6.1. Evaluation Update rule

Fully-connected networks was used to train model and evaluate the hyper-parameters. In addition to implementing fully-connected networks of arbitrary depth, I explored different update rule and "rmsprop" update rules provide the best accuracy for sand-stone only data set shown in Fig.7.

6.2. Effect of spacial variation

Using data set of sandstone, data set with or without full variation of spacial resolution are used for train the FCN model. Validation accuracy increased from 0.83 to 0.93 when the variation of spacial resolution was added to data set.

Table 2. Best validation accuracy of model trained on 6400 images for 4 classes

Model	Validation Accuracy
FCN	0.81
CNN	0.83

7. Future work

It will worthwhile to try to build the fully convolutional network architecture [5]. And, according LeCun *et al.* (2015) [3], the pretrained CNNs on other image dataset like ImageNet are still powerful to extract useful hierarchical information for images, future direction will utilize AlexNet [2] as pretrained CNN layers to extract features and compare the validation accuracy.

References

[1] J. W. Grate, M. G. Warner, J. W. Pittman, K. J. Dehoff, T. W. Wietsma, C. Zhang, and M. Oostrom. Silane modification of glass and silica surfaces to obtain equally oil-wet surfaces in glass-covered silicon micromodel applications. *Water Resources Research*, 49(8):4724–4729, aug 2013.

[2] A. Krizhevsky, I. Sutskever, and G. E. Hinton. Imagenet classification with deep convolutional neural networks. In F. Pereira, C. J. C. Burges, L. Bottou, and K. Q. Weinberger, editors, *Advances in Neural Information Processing Systems 25*, pages 1097–1105. Curran Associates, Inc., 2012.

[3] Y. LeCun, Y. Bengio, and G. Hinton. Deep learning. *Nature*, 521(7553):436–444, may 2015.

[4] L. Mosser, O. Dubrule, and M. J. Blunt. Reconstruction of three-dimensional porous media using generative adversarial neural networks. *CoRR*, abs/1704.03225, 2017.

[5] E. Shelhamer, J. Long, and T. Darrell. Fully Convolutional Networks for Semantic Segmentation. *IEEE Transactions on Pattern Analysis and Machine Intelligence*, 39(4):640–651, 2017.

[6] D. Sinton. Energy: the microfluidic frontier. *Lab On A chip*, 14(17):3127–3134, 2014.

[7] W. Yun, C. M. Ross, S. Roman, and A. R. Kovscek. Creation of a dual-porosity and dual-depth micromodel for the study of multiphase flow in complex porous media. *Lab on a Chip*, 17(8):1462–1474, 2017.

[8] B. Zhao, C. W. MacMinn, and R. Juanes. Wettability control on multiphase flow in patterned microfluidics. *Proceedings of the National Academy of Sciences of the United States of America*, 113(37):10251–6, sep 2016.